Subseasonal extremes of precipitation and active-break cycles of the Indian summer monsoon in a climate change scenario

By A. G. TURNER*, and J. M. SLINGO
Walker Institute, University of Reading, UK

(submitted 23 January 2008, revised 26 September 2008)

Summary

Changes to the behaviour of subseasonal precipitation extremes and active-break cycles of the Indian summer monsoon are assessed in this study using pre-industrial and $2 \times CO_2$ integrations of the HadCM3 coupled GCM, which is able to reasonably simulate the monsoon seasonal cycle. At $2 \times CO_2$, mean summer rainfall increases slightly, especially over central and northern India. The mean intensity of daily precipitation during the monsoon is found to increase consistent with fewer wet days, and there are increases to heavy rain events beyond changes in the mean alone. The chance of reaching particular thresholds of heavy rainfall is found to approximately double over northern India, increasing the likelihood of damaging floods on a seasonal basis. The local distribution of such projections is uncertain, however, given the large spread in mean monsoon rainfall change and associated extremes amongst even the most recent coupled climate models. The measured increase of the heaviest precipitation events over India is found to be broadly in-line with the degree of atmospheric warming and associated increases in specific humidity, lending a degree of predictability to changes in rainfall extremes. Active-break cycles of the Indian summer monsoon, important particularly due to their effect on agricultural output, are shown to be reasonably represented in HadCM3, in particular with some degree of northward propagation. We note an intensification of both active and break events, particularly when measured against the annual cycle, although there is no suggestion of any change to the duration or likelihood of monsoon breaks.

This is a preprint of an article published in the Q. J. R. Meteorol. Soc. 135, 640, pgs 549-567.
http://dx.doi.org/doi:10.1002/qj.401
http://onlinelibrary.wiley.com/doi/10.1002/qj.401/abstract

Keywords: Asian summer monsoon; global warming; rainfall extremes; intraseasonal oscillation; active-break events

1. Introduction

The Indian summer monsoon acts to tie the lives of millions of people across South Asia to the seasonal cycle, through their dependence on its rainfall for agriculture and, increasingly, industrial development. Climate change studies focusing on the monsoon have generally considered how robust the monsoon will be in the changing global climate. However, variations in the monsoon on subseasonal timescales are arguably of more importance to the local population. Short periods of heavy rainfall can cause floods with devastating consequences. In late July 2005 for example, Mumbai (Bombay) received nearly one metre of rainfall (Lal *et al.*, 2006), leading to extensive damage to infrastructure, disease, and loss of life. On the other hand, the extended monsoon break of July 2002 contributed to a country-wide drought, with All-India rainfall for the summer reaching only 81% of its long period average (Annamalai *et al.*, 2007). This led to a reduction in both agricultural output and economic growth.

In describing the impact of increased greenhouse gas forcing experiments on the Asian summer monsoon, Turner *et al.* (2007) cited several studies which noted that the monsoon remained generally robust. At $2 \times CO_2$, increases in mean Indian monsoon precipitation of 0.5–$2\mathrm{mm/day}$ were noted over India and the Bay of Bengal. A slight northward displacement of the south-westerly jet was also noted by Turner *et al.* (2007) using HadCM3, together with higher interannual variability. Both studies attributed increases in monsoon precipitation to the warmer Indian Ocean providing additional moisture. There was also a limited increase to the south-westerly flow over the northern

* Corresponding author: Walker Institute for Climate System Research, Department of Meteorology, University of Reading, PO Box 243, Earley Gate, Reading, RG6 6BB, UK. email: a.g.turner@rdg.ac.uk

Arabian Sea in Turner *et al.* (2007), attributable to the increased land-sea temperature contrast at $2 \times CO_2$. While Hu *et al.* (2000) noted increased precipitation over only peninsular India, Ashrit *et al.* (2003) saw increases over the drier regions of the northwest and far south, and others noted overall intensification of the mean pattern (Kitoh *et al.*, 1997; May, 2004). Sometimes such increases in monsoon precipitation were even in regions of weaker monsoon flow regimes (Kitoh *et al.*, 1997; Meehl *et al.*, 2000; Ashrit *et al.*, 2003), highlighting the model-dependent response of the monsoon to increased greenhouse gas forcing. In a study of the CMIP3 archive (Coupled Model Intercomparison Project data archived at the Program for Climate Model Diagnosis and Intercomparison; PCMDI), Annamalai *et al.* (2007) noted that of the six models which reasonably simulated the present day seasonal cycle of precipitation in the Indian region, all featured increased monsoon rainfall at doubled CO_2. The Intergovernmental Panel for Climate Change (IPCC) Fourth Assessment report also suggests future increases in precipitation of the Asian summer monsoon (Meehl *et al.*, 2007), although the multi-model ensemble mean response is smaller than the inter-model standard deviation.

Even with an apparently robust monsoon under increased greenhouse gas forcing, changes to the intensity of extreme events and the duration of drought spells could have much more devastating consequences, note Allen and Ingram (2002). While these authors suggest that global mean precipitation increases are constrained by the balance between radiative and latent heating, they propose that the heaviest rainfall events occur when all moisture in the column precipitates out.

The increased magnitude of these extreme events should be predictable according to the available moisture ($i.e.$, Clausius-Clapeyron) at a rate approximating $6.5\%\mathrm{K}^{-1}$ in their study. Trenberth *et al.* (2003) subsequently noted that in warmer climates where atmospheric moisture is rising more quickly than the global mean precipitation amount, increases in rainfall intensity must be offset by decreases in frequency and/or by decreased light to moderate amounts of rainfall.

To help understand how these characteristics may change in the future, we first review studies based on the recent observed record. Sen Roy and Balling Jr. (2004) studied 1910–2000 raingauge data from 129 stations spread across India, and considered seven indices measuring extreme heavy rainfall events (including largest daily rainfall totals and upper precipitation percentiles), giving a total of 903 timeseries. Of these, 61% showed an upward trend, 114 being significant. 61 timeseries had a significant downward trend. Increases were generally found spanning northwest Himalaya to peninsular India, whilst decreases were noted over the East Gangetic Plains. Goswami *et al.* (2006) puzzled over the apparent stability of precipitation over 1951–2000 from the India Meteorological Department (IMD) gridded dataset, given the rise in global surface temperatures over the same period. Focusing on the central Indian region, they noted significant rising trends in the frequency and magnitude of extreme rainfall events, and conversely a decreasing trend in the frequency of moderate events. Such compensatory changes led to little climate change signal in seasonal mean rainfall. Extrapolating such trends with further increases in greenhouse gas forcing would lead to increased flood hazards over central India in the future, conclude Goswami *et al.* (2006).

When periods of heavy rainfall last for several days, they may be thought of as active events of the monsoon. Break events form the opposing phase of this cycle of intraseasonal oscillation and can have severe impacts on agriculture, particularly if they extend for a week or more. Krishnamurthy and Shukla (2000) give a thorough account of the phenomenology of active-break cycles over the Indian subcontinent based on gridded rainfall data prepared from 3700 stations. Highlighting the importance of understanding interactions between seasonal mean rainfall and active-break events, they find that heavy drought years feature negative rainfall anomalies covering nearly all of India and persisting for the entire season. Classifying active and break events according to All-India rainfall, Krishnamurthy and Shukla (2000) note active (break) phases to feature above (below) normal precipitation over central India and below (above) normal over northern India towards the Himalyan foothills, and southern India. When atmospheric fields are studied over larger scales however, more features emerge. Annamalai and Slingo (2001) composited outgoing longwave radiation (OLR) anomalies from ECMWF reanalysis data 1979-95 based on All-India rainfall data. They noted peak power in two time bands (10–20 and 40–60 day), explaining 25% and 66% of total intraseasonal variability respectively. During active events, the authors found enhanced convection over the Indian subcontinent, extending into the Bay of Bengal and south-eastward down to the Maritime Continent and equatorial west Pacific. Reduced convection to the south of India and in the East China Sea completes a quadrupole pattern of coherent anomalies. The 10–20 day mode was noted to be on a smaller scale however. Goswami and Xavier (2005) also noticed the difference in zonal scale of the different modes, being quite narrow at 10–20 days and much broader on longer timescales (30–90 days) in their study of

NCEP-NCAR zonal wind reanalysis data at $850\mathrm{hPa}$. They also highlight propagation directions, noting the 10–20 day mode to feature westward propagation at Indian latitudes, whilst the 30–90 day mode depicts northward propagation. In their principal oscillation pattern (POP) analysis, Annamalai and Slingo (2001) also note the northward propagation of the long-period mode, highlighting its origins over the equatorial Indian Ocean. Thus active-break cycles can be considered as a component of boreal summer intraseasonal oscillations (BSISO Kemball-Cook and Wang, 2001; Fu *et al.*, 2003, and many others) involving complex interactions between northward and westward propagations, often accompanied by eastward progressions in the equatorial Indian Ocean which are of similar character to the Madden-Julian Oscillation (MJO).

In a more recent study based on 70 years of high resolution gridded rainfall data from the IMD, Krishnamurthy and Shukla (2007) instead envisage the propagation of active-break anomalies over India as southwest to northeast transitions of the monsoon trough from its preferred position over central India to the Himalayan foothills. Then, on shorter timescales, westward movement of monsoon depressions occurs within the trough itself. Providing a more detailed description than their earlier study, they describe active events beginning over the Western Ghats and east-central India, intensifying and expanding to cover the whole of central and parts of north India. Meanwhile negative precipitation anomalies reach towards the Himalaya and exist separately in the south eastern states. The final phase of the event sees positive anomalies moving toward the Himalayan foothills while the south peninsula is covered by reduced precipitation. In a subsequent study, Krishnamurthy and Shukla (2008) describe a direct relationship between the variability of convection over the broad Indian domain and rainfall over India itself.

In the observed record, disagreement in changes to active-break cycles is noted between several studies. Joseph and Simon (2005) describe the duration of break periods as increasing by 30% over the 1950–2002 period using $850\mathrm{hPa}$ zonal flow from the NCEP-NCAR reanalysis. However here they define duration as the *number* of break days in the season, neglecting their consecutive behaviour. Using raingauge data provided by the Indian Institute for Tropical Meteorology (IITM) and defining break (active) thresholds as $p < 8\mathrm{mm/day}$ ($p > 12\mathrm{mm/day}$), they note changes in number of $+45\%$ and -78% respectively. Rajeevan *et al.* (2006) however, in their study of 1° gridded data from 1951–2003, showed no significant trends in the number of active and break days in the season. This perhaps relates to their definition of events relative to standardised rainfall anomalies. In one of the few modelling studies, Mandke *et al.* (2007) study 10 coupled GCMs in the CMIP3 database, but confine their study to six, based on their present day simulation of the seasonal cycle. They define events based on precipitation over central and northwest India, and demonstrate that the response to climate change is uncertain among the models and even between 1pctto2x and 1pctto4x experiments for a given model. Some models measured showed increases in the number of active days whilst other showed decreases, however the intensity of break events and their spatial extent are shown to increase in all (some) of the models tested at $4 \times \mathrm{CO_2}$ ($2 \times \mathrm{CO_2}$). Relatively few studies have attempted to measure changes to active-break events in greenhouse gas forced GCM experiments, perhaps relating to doubts over the ability of GCMs to simulate the seasonal cycle of precipitation and features on regional scale. This paper aims to consider the impact of increased greenhouse gas forcing on intraseasonal monsoon variability in the Hadley Centre coupled GCM (HadCM3), characterized by both precipitation extremes on subseasonal timescales and active-break cycles together. This will provide a framework from which future, better resolved models, may be examined. Section 2 describes the datasets and model integrations studied, together with the choice of index used to define active and break events. In section 3, the modelled monsoon climate, its seasonal cycle and BSISO behaviour are compared with observed data. Section 4 shows how climate change manifests itself onto extremes of monsoon precipitation and the effect of increased greenhouse gas forcing on active-break cycles of the monsoon. Conclusions are drawn in section 5.

2. Method and data

(*a*) *Model integrations*

The UK Met Office Unified Model HadCM3 is used in this study, comprising fully coupled atmosphere and ocean components (Pope *et al.*, 2000; Gordon *et al.*, 2000) which exchange information once per day. The model features a stable mean state over several centuries, requiring no input of artificial heat flux adjustments at the ocean surface to combat climate drift (Johns *et al.*, 2003). While

a previous study (Turner *et al.*, 2005) found that use of an annual cycle of equatorial Indo-Pacific heat flux adjustments could improve the behaviour of monsoon interannual variability and its interaction with ENSO in this model, no improvements were found in monsoon intraseasonal variability and so they have not been employed here. The atmosphere is solved on a 3.75° longitude by 2.5° latitude grid, and as in previous studies by the authors, the atmospheric component has been run with 30 levels in the vertical rather than the standard 19 (giving higher resolution in the mid-troposphere), due to better representation of intraseasonal tropical convection such as the MJO (Inness *et al.*, 2001) and a more accurate precipitation response to high SST forcing ($e.g.$ El Niño, Spencer and Slingo, 2003). The ocean resolution is 1.25° in the horizontal with 20 vertical levels. HadCM3 provides an accurate simulation of the spatial structure of the monsoon and its seasonality (Martin *et al.*, 2000) as well as good representation of the monsoon trough (Johns *et al.*, 2003), important for simulating variations on subseasonal timescales. In addition, it was used extensively for climate change studies cited in the IPCC Third and Fourth Assessment Reports. Indeed of 18 models from the CMIP3 database which Annamalai *et al.* (2007) tested, HadCM3 was one of only 6 judged to reasonably simulate the present day seasonal cycle of the monsoon.

This study uses results from a control run of HadCM3 with pre-industrial greenhouse gas forcing (approximately $290\mathrm{p.p.m.}$, hereafter $1 \times \mathrm{CO_2}$), initialised from a previous L19 integration. An initial period of 10 years was discarded to allow for any spin-up to the increased vertical resolution, before a further 100-year integration was performed. The climate change experiment was initialised from an existing 150-year $2 \times \mathrm{CO_2}$ run, prior to which carbon dioxide had been ramped up at a rate of $1\%/\mathrm{year}$ for 70 years, in accordance with IPCC guidelines. The first 10 years of the new experiment were again discarded as a cautious adaptation to L30, before a 100 year integration at $2 \times \mathrm{CO_2}$ ($580\mathrm{p.p.m.}$) was performed. No sulphate forcing was employed.

(*b*) *Observed data*

In order to briefly validate the model used, three datasets have been obtained for comparison. The Climate Data Center Merged Analysis of Precipitation (CMAP, Xie and Arkin, 1997) has been used to assess mean precipitation. This consists of a combination of satellite and gauge data over the period 1979–2004 with monthly output. An entirely observational dataset has also been used. The India Meteorological Department (IMD) have developed a 1°-gridded dataset based on spatial averaging of station data. The original dataset (Rajeevan *et al.*, 2006) took information based on 1803 stations for the period 1951–2003, with each station available for at least 90% of days over that period. However in these data the station density over the northern plains was low. Here, a new version of the dataset is used (M. Rajeevan, personal communication, 2007), comprising 2140 stations (mainly increasing density over the northern plains) and extension to 2004. The advantage of these data is that they are daily and thus well suited for comparison with the model seasonal cycle. In addition, to study daily characteristics over the broad Indian Ocean domain, the Global Precipitation Climatology Project 1°-gridded daily dataset (Huffman *et al.*, 2001; Adler *et al.*, 2003) has been used. This covers only the recent period 1997–2007.

(*c*) *Choice of active-break index*

Many different indices have been used to generate composite evolutions of active-break events during the Indian summer monsoon. Perhaps due to the poor availability of quality long-period precipitation data, several studies based their indices on circulation obtained from reanalysis products. Goswami and Mohan (2001) recognised the stronger monsoon trough during active periods and inferred that westerlies south of the trough would strengthen during such events. They based their index on 30–60-day filtered $850\mathrm{hPa}$ zonal winds at $90^\circ\mathrm{E}, 15^\circ\mathrm{N}$, although their results were not too dependent on the exact point chosen. Webster *et al.* (1998) too chose a zonal wind-based index over the north Bay of Bengal, and selected active (break) events outside absolute anomaly values of $(-)3\mathrm{ms}^{-1}$. Goswami and Mohan (2001) however chose events based on standard deviations from the mean.

The proliferation of satellite data means that good OLR datasets are available for use as proxies for convection. Vecchi and Harrison (2002) devised a monsoon break index based on the difference between normalized 7-day boxcar smoothed OLR anomalies between two regions: Indian (10–$30^\circ\mathrm{N}$, 65–$85^\circ\mathrm{E}$) and eastern equatorial Indian Ocean ($10^\circ\mathrm{S}$–$5^\circ\mathrm{N}$, 75–$95^\circ\mathrm{E}$). The 50-day smoothed anomaly was also removed to reduce the effect of prevailing large-scale monsoon conditions on the resultant composites. Their index naturally captures the dipole of convection between the oceanic TCZ region

and Indian latitudes, and the transition and northward movement of convection between them during active-break cycles.

Precipitation, however, offers more insight into monsoon activity at the surface and its impact on the local population. Some authors average precipitation over central India, representing the core monsoon region ($e.g.$ Mandke *et al.*, 2007, uses 73–82°E, 18–28°N) due to the presence of the largest anomalies on intraseasonal timescales over this region, while opposite signed anomalies lie to the northeast and southeast. A similar region is chosen by Goswami *et al.* (2006) to represent central India (74.5–86.5°E, 16.5–26.5°N). Krishnamurthy and Shukla (2000, 2007) however chose events based on rainfall over the all-India region. Area-averaged precipitation over the Indian land surface has its climatological seasonal cycle removed before being normalized by its standard deviation. Active events exceed $+1\sigma$ while break events fall below -1σ, each for 3 or more consecutive days (5 or more in their 2007 paper). One may argue that the northward propagating nature of such events precludes using data from the whole country, however the All-India index still captures the dominant signal from the core monsoon region where seasonal mean rainfall and its anomalies are at their largest. In any case, Krishnamurthy and Shukla (2007) still demonstrate northward propagation of precipitation anomalies across India in the observed record. Additionally Annamalai and Slingo (2001) generated OLR composites based on All-India rainfall, and showed that coherent convective structures exist on a much broader scale than India, confirming that active-break events do not need to be defined in such small regions.

For model data available at the horizontal resolution of HadCM3, using data from all-India has the benefit that more data points are considered compared to a smaller region. In this study, the gridpoints were chosen after Gadgil and Sajani (1998), representing the 27 Indian land-surface points within 10–27.5°N, 71.25–86.25°E. Thus model data are averaged over the chosen gridpoints and the seasonal cycle is removed, leaving the anomalous rainfall at year y and day d as p':

$$p'(y,d) = p(y,d) - \frac{1}{100}\sum_{y=1}^{100} p(y,d). \tag{1}$$

These data are then normalized by the cycle of standard deviation through the season. Composite active and break cycles are chosen where the index exceeds $\pm 1\sigma$ for five or more days.

3. Model simulation of monsoon rainfall

(*a*) *Mean, seasonal cycle and probability distribution*

Before measuring if subseasonal extremes of monsoon variability and active-break cycles will change in the future, we perform a short validation of the simulated monsoon climate in HadCM3, its seasonal cycle, and how these may change in the future.

Figure 1 shows the seasonal mean (June to September) monsoon rainfall in HadCM3, compared with satellite derived data (CMAP, 1979-2004) and 1°-gridded IMD gauge data (1951–2004). The general precipitation climate of the northern Indian Ocean region in HadCM3 is good in comparison with CMAP, although the maximum in the eastern equatorial Indian Ocean extends too far to the south-east, and is too dry at 60°E. The simulated distribution over India and the Bay of Bengal is reasonable. Differences between the model and CMAP are no larger than those between CMAP and IMD. The IMD dataset benefits particularly from its high resolution, allowing intense rainfall upstream of the Western Ghats to be well captured, together with the downstream rain shadow. The low-level monsoon wind climatology of HadCM3 is good, if a little strong, as already described in Turner *et al.* (2005). Fig. 1d shows the climate change response of summer monsoon precipitation to CO_2 doubling. Turner *et al.* (2007) have already noted these significant precipitation increases across north India, the head of the Bay of Bengal and also the Indian Ocean off southern India, a spatial distribution well resembling that in the study of Meehl and Arblaster (2003) using the Parallel Climate Model (PCM). In HadCM3, these increases amount to around 5% when summed over the broad South Asia region (Turner *et al.*, 2007), and are made up largely by increases in convective rainfall (not shown). This is in agreement with local thermodynamic influences on increases in tropical monsoon precipitation in the multi-model ensemble of future climate integrations in the CMIP3 database assessed by Sun *et al.* (2007).

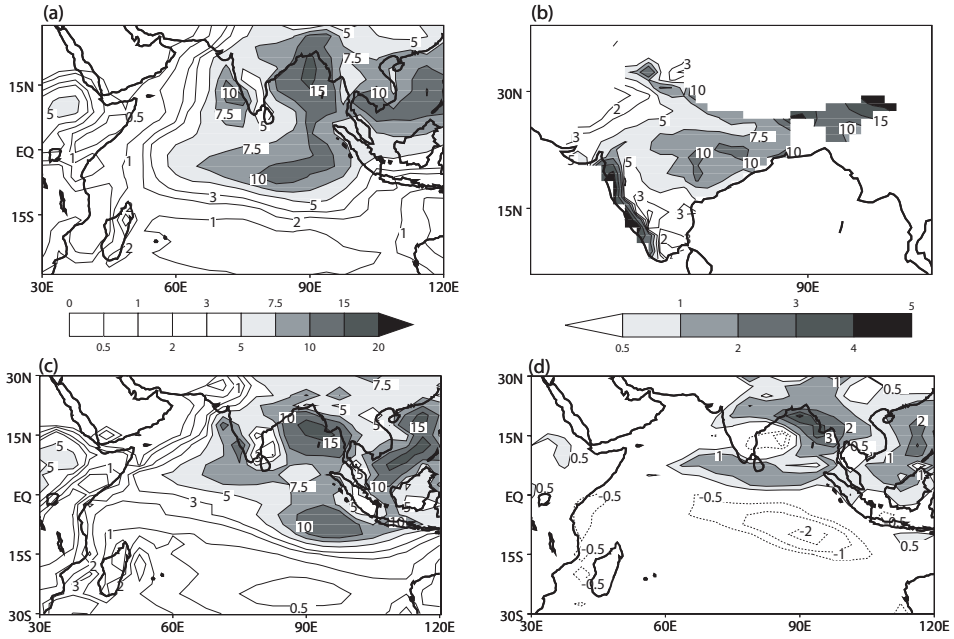

Figure 1. Seasonal mean summer (JJAS) precipitation climatology in (a) CMAP, (b) IMD gridded data, (c) HadCM3 $1 \times CO_2$ and (d) HadCM3 $2 \times CO_2$ minus $1 \times CO_2$. Units are $\mathrm{mm/day}$. Left colour-bar is for the mean climate panels (shaded only when exceeds $5\mathrm{mm/day}$), right colour-bar is for climate difference panel (positive contours solid, negative contours dashed).

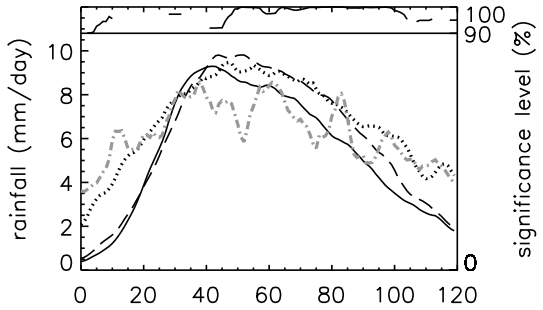

Figure 2. Mean seasonal cycle for days since June 1 in the IMD gridded dataset (dotted), HadCM3 $1 \times CO_2$ (solid) and HadCM3 $2 \times CO_2$ (dashed). Also shown for comparison are the GPCP daily data interpolated to the HadCM3 grid (grey dot-dashed). Units are $\mathrm{mm/day}$. Right-hand axis and top section show the significance level of the difference between $2 \times CO_2$ and $1 \times CO_2$ curves using a student t-test, values below 90% are omitted. Curves are smoothed using a five day running mean for clarity.

To determine when during the season these changes are occurring and for validation, the climatological seasonal cycle is presented in Fig. 2. For the model, this is determined by area-averaging precipitation over the Indian land surface (as defined in section 2.3). For the spatial mean of IMD data we first remove the detached northeastern states (Assam etc.) as these are not included in the HadCM3 mean. HadCM3 does quite a reasonable job of simulating the seasonal cycle of the monsoon as mentioned in the introduction. The two main discrepancies are the late onset in HadCM3 (around two weeks) and deficient rainfall following the peak in mid-July through to the withdrawal. As an alternative, Fig. 2 also shows a comparison against that calculated from the satellite-derived GPCP daily data 1997–2007, which has been interpolated to the model grid such that exactly the same points are used to represent Indian rainfall. This comparison reveals the weak onset and withdrawal to be robust errors in HadCM3, however rainfall during the peak period is lower than HadCM3, with wide variability in the GPCP curve reflecting the short data-period of this record. It is worth noting that the monsoon seasonal cycle of HadCM3 compares very well against 5 other models of the CMIP3 database, chosen due to their good representation of the spatial mean during the summer season (Annamalai *et al.*, 2007, their Fig. 1h). The overall weak bias of the seasonal cycle reflects subtleties in the spatial distribution of monsoon rainfall, as Turner *et al.* (2007) found HadCM3 to have a negative precipitation bias against observations over India itself, yet a positive bias when measured

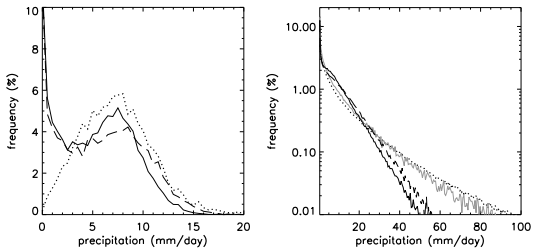

(a) (b)

Figure 3. Probability distribution functions of (a) area-averaged Indian rainfall and (b) Indian rainfall with no spatial averaging in the IMD gridded dataset (dotted), HadCM3 $1 \times CO_2$ (solid) and HadCM3 $2 \times CO_2$ (dashed). In (b), grey curve shows IMD data when downgraded to the $\mathrm{N48}$ grid of HadCM3. Bins are $0.5\mathrm{mm/day}$ wide.

over the broader South Asian monsoon region. Biases during the onset may inhibit intraseasonal activity during the early part of the season (Kemball-Cook and Wang, 2001). At $2 \times CO_2$, increases in daily precipitation generally occur from mid-July to late September, significant above the 95% level.

To look at the distribution of rainfall events in HadCM3, probability distribution functions (hereafter pdfs) of daily data are shown in Fig. 3. This comprises two methods: (a) a combination of all data as an area average and (b) each gridpoint. The area-average in Fig. 3a is performed over 27 model grid-points of the Indian land-surface (and all data in the IMD grid), and precipitation is divided into $0.5\mathrm{mm}$ bins. HadCM3 $1 \times CO_2$ simulates the gross features of the rainfall distribution, with the most likely daily precipitation total being around $8\mathrm{mm}$ in model and observations. However, at low rainfall amounts the curves reveal a high degree of spatial coherence in HadCM3. That is, when it drizzles in HadCM3 it is often doing so over the whole subcontinent. IMD is based on station data and provides a better representation of small-scale convective events in response to India's varied orography, versus smoother orography and convection in HadCM3. Precipitation is thus more inhomogeneous over India in nature, reducing the count to zero at low values.

A simple skill score to test the common area between two pdf curves was devised by Perkins *et al.* (2007), and is reproduced here:

$$S_{\mathrm{score}} = \sum_{1}^{n} \min(f_{\mathrm{obs}}, f_{\mathrm{mod}}), \tag{2}$$

where the score is summed over all n bins, and f_{obs}, f_{mod} are the precipitation frequencies for a given bin in the observations and model respectively. Values of S_{score} approaching 1 indicate a high skill in simulating the distribution of precipitation. Comparing the IMD and HadCM3 $1 \times CO_2$ curves in Fig. 3a, we have $S_{\mathrm{score}} = 0.77$, which is quite reasonable (and above the cutoff which Perkins *et al.*, 2007, use to discard poorly-performing models in their study of Australian rainfall).

Alternatively, Fig. 3b shows rainfall pdfs for all grid-points with no spatial averaging and on a log-frequency scale, allowing for improved interpretation at high rain rates. Here the $1 \times CO_2$ model curve is similar to that of the IMD gridded data, including a very high frequency of drizzle. Sun *et al.* (2006) noted too frequent precipitation at low intensity to be a common problem amongst GCMs (after Dai and Trenberth, 2004). This is in part related to the gridding, which increases precipitation frequency at the expense of reduced intensity. Hennessy *et al.* (1997) pointed out that one would expect GCMs to underestimate the frequency of heavy convective precipitation (as in the monsoon), because this occurs on sub-grid scales and is thus being spread over a larger area in HadCM3. Sun *et al.* (2006), however, demonstrated that the difference between grids of 1° (IMD) and 3° (HadCM3, approximately) were small compared to differences between models, or between gridded and station data. It is clear from Fig. 3b that, when looking at grid-points separately, HadCM3 is overestimating moderate rainfall at the expense of events in the upper tail. To test the effect of the grid size itself, the grey curve in Fig. 3b represents the IMD data downgraded to the HadCM3 grid. This is achieved by extrapolating IMD data over missing ocean regions (the Arabian Sea and Bay of Bengal) before bi-linearly interpolating to the $3.75^\circ \times 2.5^\circ$ spacing of HadCM3. The same 27 Indian land-surface grid points are selected as in HadCM3, reducing the number of points from 357 to 27 and causing increased noise in the tail. There is clear evidence of a reduction in precipitation intensity in the upper tail due to data gridding alone.

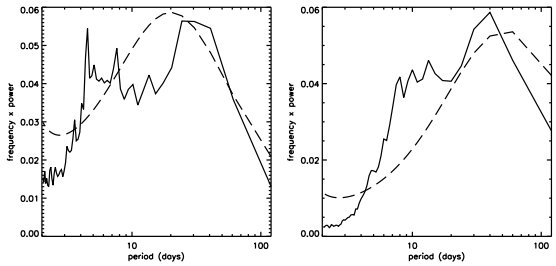

Figure 4. Normalized power spectra of daily rainfall anomalies averaged over the Indian region in (a) IMD gridded data, excluding the far northeast states and (b) HadCM3 $1 \times CO_2$. Spectra are calculated for each JJAS season separately before being smoothed using a Tukey window. The theoretical spectra of an AR(1) process (first-order autoregressive) are used to distinguish peaks from red noise.

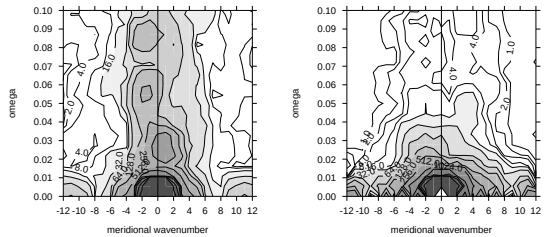

Figure 5. Space-time spectra on 2–128 day filtered precipitation anomalies in (left) GPCP and right (HadCM3) over the domain 70–100°E, 30°N–30°S. Contours are powers of two, those above 16 are shaded.

Both parts of Fig. 3 suggest that at doubled CO_2, there is a decreased probability of moderate rainfall, compensated for by increases in heavy rainfall events, particularly in the upper tail. This is consistent with the study of Semenov and Bengtsson (2002) who noted increased heavy precipitation at the expense of lower intensities in their IS92a scenario of the ECHAM4/OPYC3 model combination. Similarly, Hennessy *et al.* (1997) noted a general decreased probability of moderate rainfall against increased frequencies at low and heavy levels. The largest increases in their study of two coarse-resolution slab-ocean models were for very heavy rainfall.

(*b*) *Evidence for BSISO*

In order to later examine changes to active-break cycles of the monsoon in HadCM3, here we briefly validate intraseasonal behaviour during the boreal summer (BSISO) and discuss some of the inherent biases in the model. Figure 4 shows normalized power spectra for the daily all-India rainfall spatially-averaged over the IMD grid or Indian land surface gridpoints in HadCM3 (see section 2.3). The spectra are calculated over each JJAS season separately before an average is taken. In HadCM3, major significant peaks are evident at around 10–20 days and 40 days. These are broadly consistent with the periods described in studies cited in the introduction. In the IMD dataset, somewhat more 'weather noise' is evident at short periods (< 10 days), however a significant peak is noted between 30 and 40 days.

To test propagation characteristics, we calculate space-time spectra over the Indian domain during the May to October season, in order to also capture any intraseasonal variability associated with the monsoon onset and withdrawal. Data is first filtered to intraseasonal (2–128 day) timescales using a Lanczos filter (Duchon, 1979) before being zonally averaged. Then fast Fourier transforms convert rainfall data in the (y, t) domain to wavenumber-frequency space (l_y, ω). The space-time spectra shown in Fig. 5 are given by the square of the absolute value of the Fourier coefficients, averaged over each year in the datasets. As shown by the figure, northward propagation is primarily at the gravest meridional wavenumber (Lin *et al.*, 2008; Fu *et al.*, 2003) in GPCP observations. In HadCM3, northward power is not quite as distinct as in observations and concentrated at lower wavenumbers / higher frequencies, suggesting slower phase speeds. HadCM3 also lacks obvious variance in southward modes (negative meridional wavenumbers).

Finally, to demonstrate BSISO propagation more clearly we use lag-correlations of 30–60 day bandpass-filtered precipitation during the extended boreal summer (MJJASO) in the Indian domain

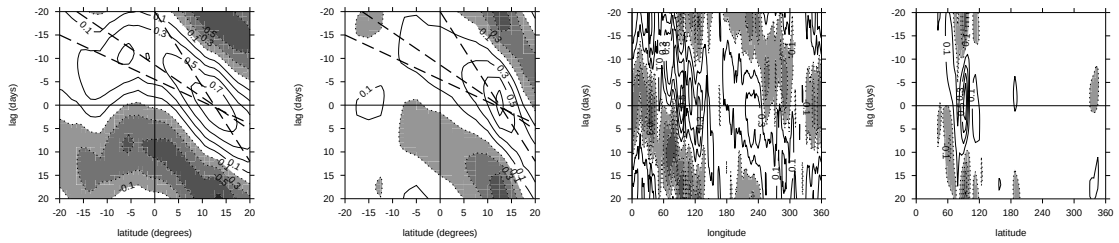

(a) (b)

Figure 6. Lag-correlations of 30–60 day filtered rainfall anomalies during May to October showing northward and eastward propagations in the Indian monsoon region after Lin *et al.* (2008): (a) zonally averaged over 70–$100^{\circ}\mathrm{E}$ against itself near $12.5^{\circ}\mathrm{N}, 85^{\circ}\mathrm{E}$, (b) meridionally averaged over 5–$25^{\circ}\mathrm{N}$ against itself near to $15^{\circ}\mathrm{N}, 95^{\circ}\mathrm{E}$. Positive contours solid, negative contours dashed and shaded. In (a), the thick dashed lines represent approximate phase velocities of 0.8, 1.8 and $2.8\mathrm{ms}^{-1}$. Shown are GPCP observations (left) and HadCM3 (right).

against some reference point. Figures 6a,b depict northward and eastward propagation respectively. We choose identical domains and reference points to Lin *et al.* (2008) so that a direct comparison can be made with the multi-model data used in their study. Figure 6a shows that HadCM3 is clearly capable of some northward propagation in the Indian domain, to a degree comparable with many of the other models in the CMIP3 database (see Lin *et al.*, 2008, Fig. 16) and GPCP observations. Also shown in the figure are lines indicating the same phase speeds as in Lin *et al.* (2008). Although they found northward propagations in GPCP to be around $1.8\mathrm{ms}^{-1}$, here the propagation seems slightly slower, perhaps due to the longer dataset used here. In HadCM3, northward propagations are slightly slower than $0.8\mathrm{ms}^{-1}$. HadCM3 also shows an absence of southward propagation from around $5^{\circ}\mathrm{S}$, although this should not affect intraseasonal activity over India itself. Both these findings are consistent with Fig. 5. To show that northward propagation is not simply a manifestation of eastward motion of a northwest-southeast tilted rainband (as implied in Fu *et al.*, 2003), Fig. 6b shows eastward propagations at Indian latitudes. These are very weak in HadCM3 when compared to GPCP data, and consistent with Lin *et al.* (2008) who showed little correspondence between northward and eastward BSISO modes in most CMIP3 models. Kemball-Cook and Wang (2001) suggested the importance of air-sea interactions over the Indian Ocean for propagations associated with the BSISO and the poor representation of these interactions in coupled models, together with weakness of the seasonal cycle during the monsoon onset (Fig. 2), may be the cause of such biases in HadCM3.

4. Results

(*a*) *Changes to precipitation extremes*

Changes to precipitation extremes can manifest themselves both in the intensity, duration, and likelihood of events. This section considers the impact of increased greenhouse gas forcing on changes in precipitation event characteristics.

A first measure of the reliability of precipitation during the monsoon season can be given by the number of wet days, or the proportion of the season in which rain occurs. In the IMD data, roughly 60% of days during the season JJAS are wet over central India, rising above 70% over the Western Ghats and 80% in the northeast, while falling to 20% in the dry north-western states, and around 30% in the southeast (not shown). Using daily Indian station data from 1986 to 1989, Stephenson *et al.* (1999) saw a range of 40–60% wet days over peninsular India and fewer over the northwest deserts. The occurrence of wet days through the monsoon season is shown for HadCM3 in Fig. 7(a). To avoid computational and truncation errors manifest in the output of model precipitation, a low precipitation cut-off of $0.1\mathrm{mm/day}$ is used to define a wet day, below which days are defined as dry (after Stephenson *et al.*, 1999; Semenov and Bengtsson, 2002). Under control conditions, HadCM3 reasonably simulates the spatial variation in occurrence of wet days, between 60–70% over much of central India and rising above 70% in the northeast and over the Western Ghats. In the southeast, the proportion of wet days during the season reaches similar levels to the observed dataset, although the signal is displaced somewhat into the Bay of Bengal. This likely reflects the coarse model resolution and poor simulation of the rain shadow east of the Western Ghats.

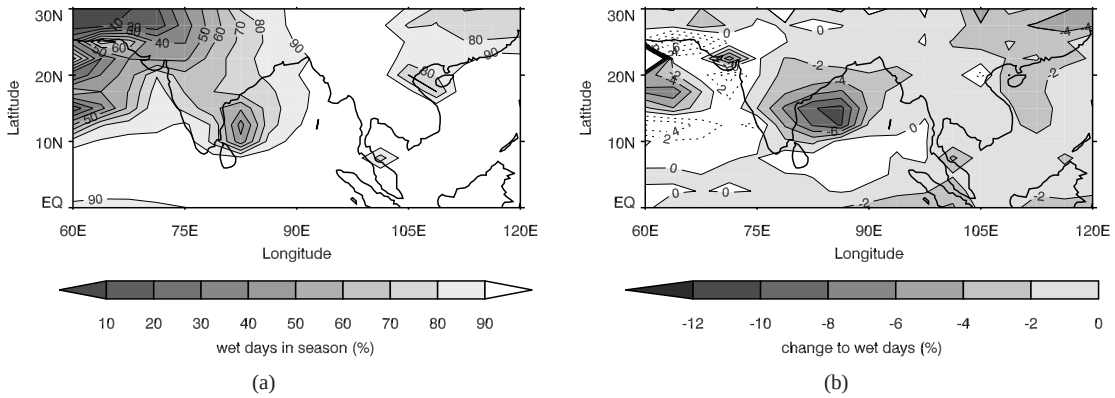

Figure 7. Percentage number of wet days per season in (a) HadCM3 $1 \times CO_2$ and (b) HadCM3 $2 \times CO_2$ minus $1 \times CO_2$. Rainfall is defined as occurring where precipitation exceeds $0.1\mathrm{mm/day}$ on a given day.

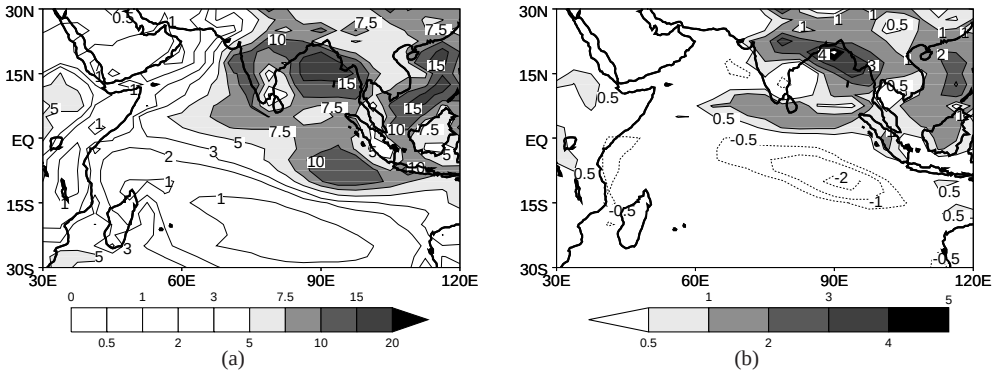

Figure 8. (a) Summer mean rainfall intensity in HadCM3 and (b) HadCM3 $2 \times CO_2$ minus $1 \times CO_2$. Rainfall is defined as occurring where precipitation exceeds $0.1\mathrm{mm/day}$ on a given day.

At $2 \times CO_2$ there are more than 2% fewer wet days per season (shown in Fig. 7(b)), amounting to an extra three days with no rainfall. This figure rises rapidly out into the southwest Bay of Bengal. Semenov and Bengtsson (2002) also noted a clear reduction in the probability of wet days occurring in the ECHAM4/OPYC3 coupled model between transient simulations of the 20th and 21st centuries.

The number of wet days can be related to the precipitation intensity, hence mean precipitation intensity is calculated as the total seasonal precipitation divided by the number of wet days in the season at each gridpoint. In observations, precipitation intensity is generally wetter for all areas of India than the corresponding seasonal mean (not shown), but is qualitatively similar. This confirms the discrete nature of rainfall events, many of which are very intense (Stephenson *et al.*, 1999). Mean precipitation intensity is shown for HadCM3 in Fig. 8a, and is seen to be qualitatively similar to (but larger in magnitude than) the corresponding seasonal mean (Fig. 1c). The model features generally reduced levels of precipitation intensity in comparison with the IMD observed data. This can be partially attributed to the coarse model grid (each gridbox in HadCM3 represents more than 9 times the area of a 1° box in the IMD data), which acts to smooth out heavy events (Sun *et al.*, 2006).

The response of precipitation intensity to increased greenhouse gas forcing is large (see Fig. 8b), especially over northern India and the north Bay of Bengal, reaching $+2$–$4\mathrm{mm/day}$. This pattern is in spatial agreement with the climate change response of mean precipitation (Fig. 1d), although intensity increases to a greater degree, especially over northern India. Given that intensity is proportional to the mean and varies inversely with the number of wet days, this finding is consistent with the decreased number of wet days seen in Fig. 7(b). The only intensity decreases noted in our study occur over south-east peninsular India, a region which features little mean change but more wet days, and in any case one of the drier regions during the Indian summer monsoon.

To examine the spatial detail of heavy rainfall events on subseasonal timescales, the levels of precipitation at heavy (defined as the 95th) and very heavy (99th) percentiles are shown in Fig. 9

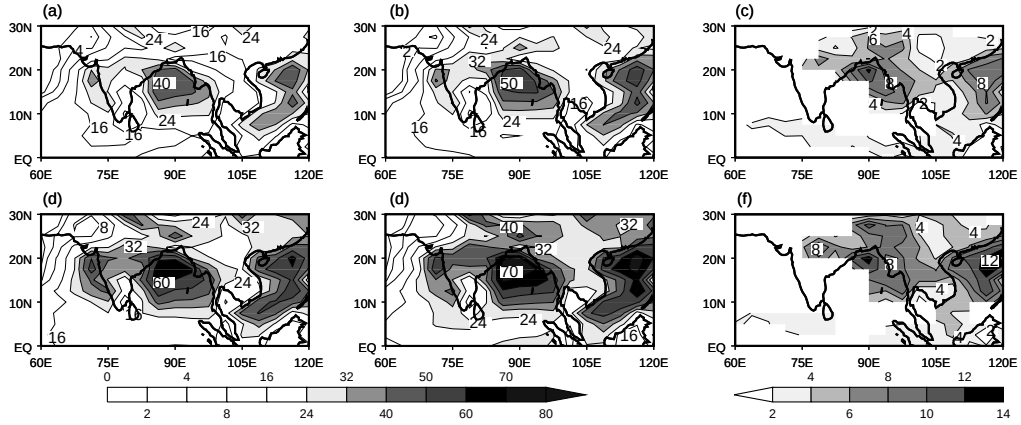

Figure 9. Spatial patterns of extreme daily rainfall at the heavy (95th percentile) level: (a) HadCM3 $1 \times CO_2$, (b) HadCM3 $2 \times CO_2$, and (c) their difference. (d) to (f) show the same but for very heavy (99th percentile) levels of precipitation. Percentiles are calculated on a season-by-season basis and the mean is taken. Absolute panels feature shading above $24\mathrm{mm/day}$, difference panels are shaded above $2\mathrm{mm/day}$. Only those differences significant above the 95% level are shown, there are no significant negative changes.

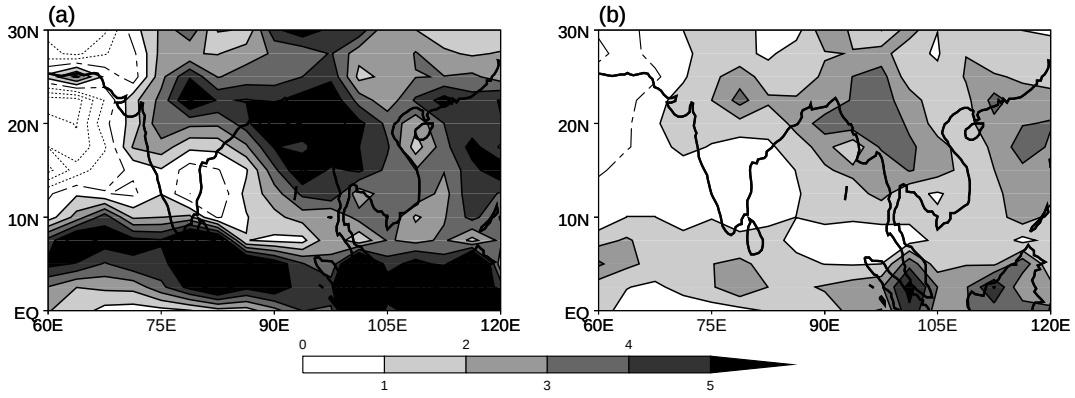

Figure 10. Percentage change in the likelihood of reaching $1 \times CO_2$ precipitation levels: (a) heavy (95th percentile) and (b) very heavy (99th percentile) as CO_2 concentrations are doubled. A 5% (1%) increase in the chance of (very) heavy rainfall amounts to a doubling, by definition.

for both climate scenarios. These levels of precipitation are exceeded on approximately 6 days and 1 day per season. To avoid the effects of interannual variability (and hence clustering of heavy rainfall in a particular year), percentiles are calculated separately for each season before the mean is taken. The differences in the levels of precipitation associated with these upper percentiles are shown in Figs. 9c,f. These indicate increased levels of heavy and very heavy precipitation at $2 \times CO_2$. Such changes are particularly marked in northern India, the Bay of Bengal and the Indochina peninsula, exceeding changes in the mean. Such increases are statistically significant above the 95% level using a student t-test (as shown in Figs. 9c,f) and even at the 99% level (not shown). At the 95th percentile (one in 20 days), events are up to $8\mathrm{mm/day}$ stronger over the northern states ($12\mathrm{mm/day}$ over Bay of Bengal).

Changes to rainfall extremes can also be interpreted by examining the probability of reaching the absolute level of a given upper percentile at $2 \times CO_2$. At $1 \times CO_2$, heavy and very heavy precipitation events are occurring on 5% and 1% of all days in the season, by definition. Figure 10 measures the increased probability of attaining these absolute levels of precipitation at $2 \times CO_2$. Heavy precipitation, as defined at $1 \times CO_2$, is up to 5% more likely over northern India during JJAS in HadCM3 $2 \times CO_2$ (Fig. 10a). As its previous likelihood was 5%, these events are thus twice as likely. Similarly, at the very heavy threshold (Fig. 10b), an increase of 2–3$\%$ over northern India suggests very heavy events are *more* than twice as likely. Hennessy *et al.* (1997) note a similar divergence in the response of event return periods to CO_2 doubling, $i.e.$, magnified probability increases further up the distribution. Kharin *et al.* (2007), however, caution that there are very large uncertainties in changes to precipitation extremes in the tropics, both amongst models integrated under the SRES scenarios for

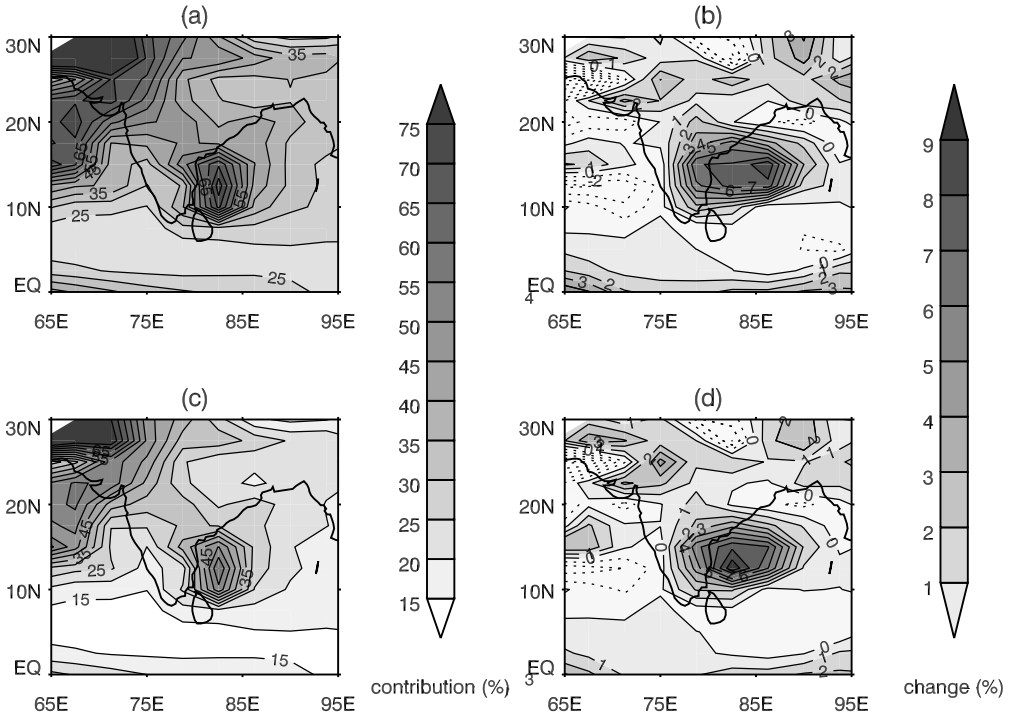

Figure 11. Spatial pattern of the percentage contribution of subseasonal precipitation extremes to seasonal mean rainfall totals: (a) contribution of moderately heavy (90th percentile) in HadCM3 $1 \times \mathrm{CO}_2$, and (b) the percentage change at $2 \times \mathrm{CO}_2$. The same is shown for heavy (95th percentile) levels of precipitation in (c) and (d).

IPCC AR4 and observed datasets. Here the spatial changes to absolute levels of the upper extremes or their probability are strongly tied to the seasonal mean changes shown earlier.

Rather than having entirely negative impacts on society, heavy precipitation, when properly harnessed, can act as the lifeblood of agriculture and industry, through irrigation systems or reservoirs storing water for HEP (hydro-electric power generation). To measure the importance of heavy precipitation events, their contribution to total seasonal rainfall is shown in Fig. 11. This is calculated on a season-by-season basis before taking the mean, as in Fig. 9, to avoid the effects of interannual variation. Rainfall above the 90th percentile contributes typically 40% of the seasonal total for much of India, and this contribution remains as high as 25% even at the 95th percentile. Looking at the issue of contribution from another angle, Sun *et al.* (2006) studied the number of days over which 67% of total annual rainfall accumulates. In their study, HadCM3 receives most of its annual total in less than 30 days, in common with most other coupled GCMs of the IPCC AR4, and broadly similar to the observed gauge and satellite data compared in their study. At $2 \times \mathrm{CO}_2$ (Figs. 11b,d), contributions from the heaviest events increase particularly over the southeast coast of peninsular India where summer mean rainfall is low (Fig. 1), indicating increased reliance on heavy precipitation for the seasonal total to be attained. This will require increased adaptation in the use of water resources in terms of management, storage, distribution, drainage etc. Together with the reduced probability of wet days illustrated in Fig. 7(b), this finding indicates a climate more prone to droughts, in agreement with the modelling study of Semenov and Bengtsson (2002). In contrast to our confined signal, in a study of trends in the observed record based on Indian station data, Alexander *et al.* (2006) have noted positive trends in the contribution of the 95th percentile to the annual total (denoted $\mathrm{R95pT}$) over most of India for the period 1951–2003. This difference may relate to the data used, or our use of seasonal instead of annual measures.

Projections of changes to subseasonal extremes in the previous figures are subject to uncertainty in their spatial distribution, tied to the projected pattern of change in the seasonal mean or the number of wet days through the season. In order to provide a bulk measure of these changes, and to summarize these results, Table 1 presents averaged values of mean precipitation intensity, upper rainfall percentiles and the change in probability of reaching a given percentile. We choose the central Indian region, after Goswami *et al.* (2006) of 74.5–$86.5^\circ\mathrm{E}$, 16.5–$26.5^\circ\mathrm{N}$. As indicated in Table 1 and Figs. 9–11, mean precipitation intensity generally increases beyond change in the mean, and extremes

TABLE 1. Rainfall characteristics for central India (74.5–86.5°E, 16.5–26.5°N) during JJAS: mean intensity, 90th, 95th and 99th percentiles (all in $\mathrm{mm/day}$), and the change in probability in reaching the $1 \times \mathrm{CO_2}$ levels associated with those percentiles (as percentage changes).

	mean intensity	extreme percentile		
		90	95	99
$1 \times \mathrm{CO_2}$	9.7	18.3	24.0	35.2
$2 \times \mathrm{CO_2}$	11.4	21.4	27.9	40.6
$2 \times \mathrm{CO_2} - 1 \times \mathrm{CO_2}$	1.73	3.11	3.93	5.92
$\Delta_{\mathrm{prob}}(1 \times \mathrm{CO_2})$	-	4.3%	3.5%	1.7%

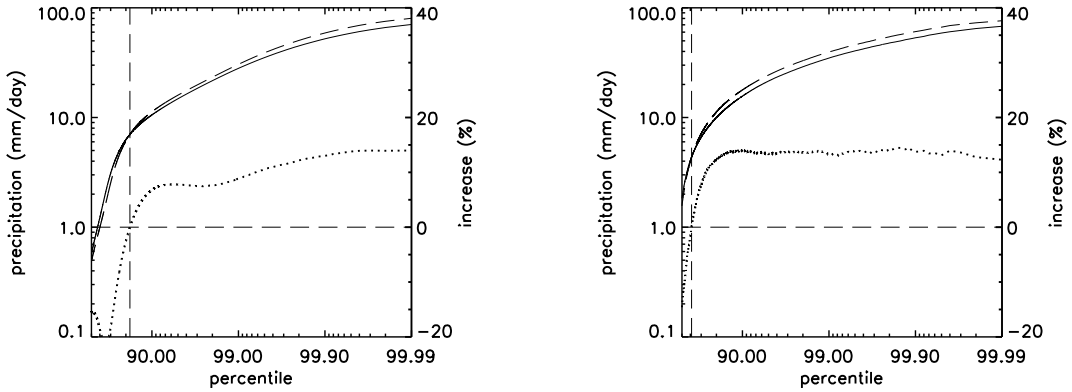

Figure 12. Levels of precipitation in the upper quartiles of (a) tropics-wide (30°N–30°S) and (b) all-India rainfall for HadCM3 $1 \times \mathrm{CO_2}$ (solid) and $2 \times \mathrm{CO_2}$ (dashed). Each gridpoint of data is used in each case (no spatial average). Ratio showing their percentage change is also shown (dotted) and measured on the right-hand axis. After Allen and Ingram (2002).

of precipitation increase even more markedly at $2 \times \mathrm{CO_2}$. The probability of attaining the $1 \times \mathrm{CO_2}$ level of precipitation associated with a given extreme also increases at $2 \times \mathrm{CO_2}$ in HadCM3 ($e.g.$, the 90th percentiles is 10% likely at $1 \times \mathrm{CO_2}$, but $10 + 4.3 = 14.3\%$ likely at $2 \times \mathrm{CO_2}$).

Finally, to look at the upper extremes of precipitation in a more detailed manner and determine if changes to them are in any way predictable, a percentile curve is constructed after Allen and Ingram (2002). The precipitation data are taken from the upper two quartiles at each gridpoint in the tropics-wide region, and at each gridpoint over the Indian land surface (as defined in Section 2.3). Figure 12 shows the level of precipitation at each of the upper percentiles at $1 \times \mathrm{CO_2}$ and $2 \times \mathrm{CO_2}$, together with their ratio. Precipitation increases at $2 \times \mathrm{CO_2}$ for all percentiles above $\sim 70\%$ in the tropics-wide case and over $\sim 60\%$ for India. The response of precipitation associated with given upper percentiles is relatively flat over India, possibly due to the smaller matrix of input data compared to the tropics-wide case; 27 grid-points $\times$ 100yr $\times$ 120 days, restricting the number of measurable data-points to ~ 32 at the 99.99% level. Maximum precipitation increases by 13–14% for both India and the wider tropics. To investigate the degree to which these increases are in-line with those predicted using the Clausius-Clapeyron equation ($e.g.$, after Allen and Ingram, 2002, who used $6.5\%\mathrm{K}^{-1}$ based on a global average temperature of 14.2°C), the climate sensitivity of the model is calculated. Defined as the equilibrium response of surface air (1.5m) temperature to $\mathrm{CO_2}$ doubling, we limit the calculation to the tropics (30°N–30°S), yielding $\Delta T = +2.27$K. The weighted mean temperature of the same region is 296.3K, yielding via Clausius-Clapeyron an increment rate of $6.05\%\mathrm{K}^{-1}$ and thus a theoretical maximum precipitation increase of $+13.7\%$. Note that Allen and Ingram (2002) saw greater increases to the magnitude of the heaviest precipitation in a different configuration of HadCM3, at around 25%. Reconsideration of the data used in that study revealed that such changes were really being measured over $2.7 \times \mathrm{CO_2}$, with its corresponding higher climare climate sensitivity (Pall *et al.*, 2007, their Fig. 1). Allen and Ingram (2002) argue that in the tropics, measured increases may be more than these predictions due to feedbacks between the release of latent heat and large-scale flows supplying moisture. This is particularly true for the India where convective latent heat release maintains the monsoon following its onset (Sperber *et al.*, 2000). However, the increases in the heaviest precipitation in HadCM3 do not outpace changes to in-situ moisture availability since

there is very little increase in the strength of the broad scale Somali Jet at $2 \times CO_2$ in this model (Turner *et al.*, 2007). These modelled changes have backing in recent observations. In their study of the IMD data, Goswami *et al.* (2006) noted an upward trend of extremes over 1950–2000, especially at the upper levels where precipitation values which constituted the 99.75 percentile during the 1950s reached only the 99.5 percentile by the early 1990s. In other modelling studies such as an IS92a emissions simulation of the 21st century using the ECHAM4/OPYC3 model combination, Semenov and Bengtsson (2002) used analysis of the Gamma distribution to show positive trends in the scale parameter, indicating stretching of the probability distribution and exponential increases in heavy events.

(*b*) *Changes to active-break cycles*

While extreme precipitation events such as those detailed above are undoubtedly important, consideration needs to be given to both phases of intraseasonal variation as part of active-break cycles of the Indian summer monsoon. Indeed one of the major unanswered questions of monsoon climate change research is the impact of increased greenhouse gas forcing on such variations. Their intensity, frequency of occurrence and duration are vitally important, especially for the sowing and harvesting of crops.

Composite active and break cycles have been constructed using the all-India rainfall index defined in section 2. Where the standardised daily rainfall anomaly exceeds one standard deviation (falls below minus one standard deviation) and persists for at least five days, an active (break) period is defined. The mid-point of each active or break period during JJAS of each dataset is defined as the lag-zero reference. Where event duration is even, the mid-point is rounded nearer to the event onset ($e.g.$, if an event lasts six days then the mid-point is day three). Using this index definition, the mean length of active (break) periods in HadCM3 is 9.3 days (10.6) versus 7.0 (7.6) using the area-average of the raw IMD data. Those years in which there are no events of at least five days are excluded from the mean. In the IMD data, the mean length of events is around 2 days shorter than in HadCM3. This possibly relates to the tendency for HadCM3 to simulate homogeneous precipitation anomalies over the whole of India, as suggested in section 3. Greater spatial heterogeneity in the observed data results in less likelihood of achieving days where all-India rainfall satisfies the active or break threshold. Model horizontal resolution is the most likely cause of this both directly ($e.g.$, imperfections in the spatial distribution of convection associated with India's varied orography) and indirectly (the IMD and HadCM3 data being on different grid resolutions).

Lag-composites of precipitation anomalies are generated for active and break periods at both $1 \times CO_2$ and $2 \times CO_2$ in HadCM3. These are shown for active event precipitation anomalies to the annual cycle in HadCM3 $1 \times CO_2$ in Fig. 13. Prior to active periods (lag-20), positive anomalies can be seen building up off the west coast of India, followed by advancement into the south peninsula (and consistent with Krishnamurthy and Shukla, 2007). These anomalies become a zonal band over much of central and southern India at lag-12, reaching an amplitude of up to $3\mathrm{mm/day}$ against the seasonal cycle. Stretching across some 30° of longitude, the band becomes more zonally uniform and begins to expand northward by lag-8. Strong intensification of the anomaly occurs by lag-4, especially west of Mumbai and in the Bay of Bengal. Around this time, a similar zonal band of negative anomalies begins to intensify further south, corresponding to reductions in convection over the equatorial TCZ region, with a minimum around $90^\circ\mathrm{E}$. This represents a dipole in active-break monsoon convection, between equatorial and Indian latitudes, which is captured in the composites despite the use of an index based solely on India. Such a dipole is seen more strongly (not shown) when using the OLR active-break index of Vecchi and Harrison (2002). As time progresses to zero-lag, anomalous precipitation is maximised over India and the Bay of Bengal, reaching $+6$–$7\mathrm{mm/day}$. Despite the chosen index measuring only Indian land-surface rainfall, the composite anomaly peaks over the Bay of Bengal, illustrating the organized zonal structure of active-break events and greater availability of moisture over the bay. Modelled patterns of precipitation around the centre of the active period resemble the quadrupole of convection noted in the observed data by Annamalai and Slingo (2001). This quadrupole consists of positive anomalies over India / Bay of Bengal and further southeast in the South China Sea / Indochina, whilst negative anomalies exist over the equatorial Indian Ocean and in a zonal band across southern China into the East China Sea. As the event progresses past maturity, the positive precipitation anomalies decline first in the Bay of Bengal and southern states (lag+4), before moving northwards and shrinking both in magnitude and zonal extent. By lag+12, anomalies largely disappear.

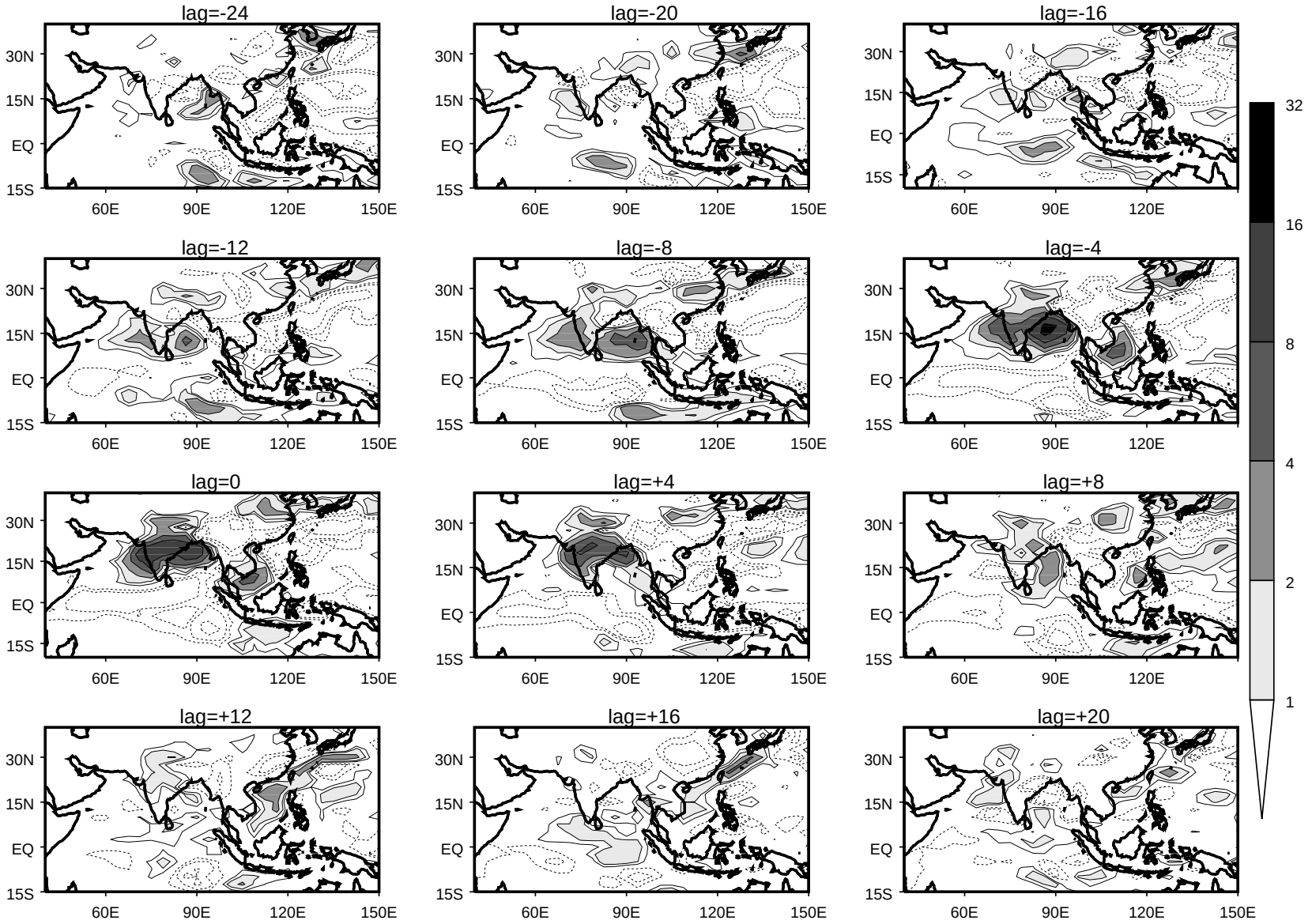

Figure 13. Lag composites of precipitation anomalies to the seasonal cycle during active events in HadCM3 $1 \times CO_2$, defined by the all-India rainfall index of section 2.3. Units are $\mathrm{mm/day}$, and lag times are given in days with respect to the centre of an event.

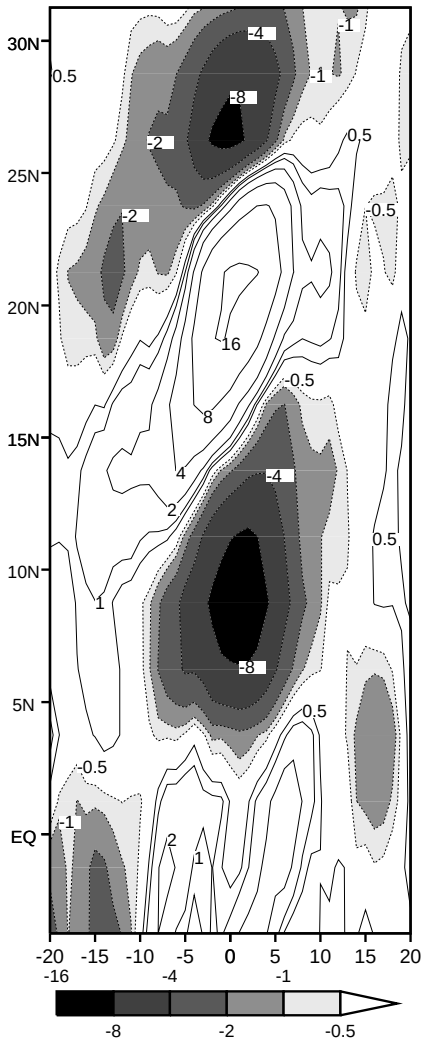

Figure 14. Hovmöller composite of anomalous active period vorticity at $850\mathrm{hPa}$ during JJAS, constructed from the active-break index defined by Fig. 13. Zonally averaged over the Indian region ($70 - -90^{\circ}\mathrm{E}$). Negative anomalies are shaded and have dashed contours whilst positive anomalies have solid lines. Units of lag (vorticity) are days ($10^{-6}\mathrm{s}^{-1}$).

Compositing over so many events of differing lengths in the 100-year dataset means that obvious indications of northward propagation can be difficult to see. However, based on the active-break precipitation index used in Fig. 13, Fig. 14 shows a Hovmöller diagram indicating northward propagation of lower-tropospheric vorticity anomalies at Indian longitudes. Cyclonic anomalies pass over the southern tip of peninsular India around 15 days before an active event, intensify, and continue moving northward until at least 10 days after the event peak. Using the positive cyclonic anomalies in Fig. 14, we calculate a phase speed of around $0.6\mathrm{ms}^{-1}$ northwards, consistent with that measured in the lag-correlations of Fig. 6.

In the break composite (not shown), anomalies evolve in an equal but opposite fashion, although around zero-lag there are less obvious extensions of the break anomaly to the South China Sea, unlike the active composites. Monsoon breaks reduce precipitation over India by around $5\mathrm{mm/day}$ during the event peak (amounting to absolute levels of only $2\mathrm{mm/day}$), and by almost $9\mathrm{mm/day}$ over the Bay of Bengal. The quadrupole structure is only visible if the active-break criteria is relaxed to $\pm 0.5\sigma$, bringing more events into the composite. Event decay is consistent with anomalies moving to the north.

To investigate the impact of increased greenhouse gas forcing on active-break cycles of the monsoon, Fig. 15 shows composites of active and break events at lag-zero. Given that the seasonal cycle is enhanced at $2 \times \mathrm{CO}_2$ (as seen in Fig. 2), absolute levels of precipitation during monsoon breaks could be broadly similar. Thus we first describe levels of absolute precipitation at $1 \times \mathrm{CO}_2$, $2 \times \mathrm{CO}_2$ and their difference (Fig. 15a,c,e for active and Fig. 15b,d,f for break events). Precipitation

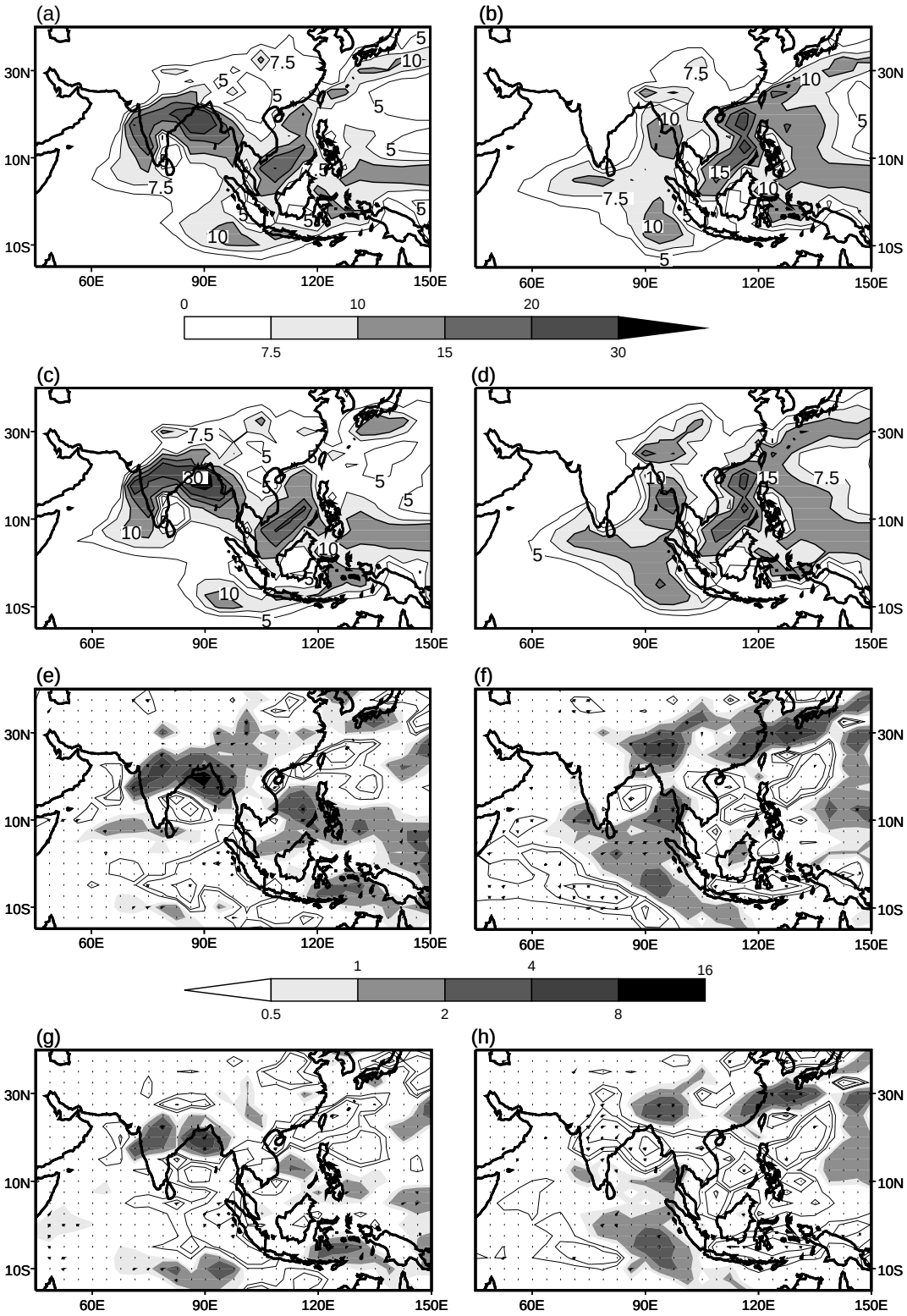

Figure 15. Absolute levels of precipitation associated with lag-zero composites of active-break cycles in HadCM3: active and break at $1 \times CO_2$ (a,b); at $2 \times CO_2$ (c,d) and their difference ($2 \times CO_2$ minus $1 \times CO_2$; e,f). Also shown are the differences between $2 \times CO_2$ and $1 \times CO_2$ active and break anomalies to the seasonal cycle (g,h). Units are $\mathrm{mm/day}$. In the difference plots, stippling indicates significance at the 95% level using a student t-test.

TABLE 2. Change in precipitation at zero-lag of active and break events averaged over the core monsoon region (Goswami *et al.*, 2006, 74.5-86.5°E, 16.5–26.5°N) in response to doubling of CO_2. Differences are shown as an absolute measure ($e.g.$, Figs. 15e,f) and when changes to the seasonal cycle are taken into account (as in Figs. 15g,h). An asterisk* indicates significance beyond the 99% level using a student t-test. Units are $\mathrm{mm/day}$.

precipitation difference	active	break
absolute	$+3.36^*$	$+0.12$
anomaly to seasonal cycle	$+2.07^*$	-1.66^*

during active events is stronger over India at $2 \times CO_2$, consistent with the arguments presented in section 4.1. Break events are not measurably more severe in absolute terms at $2 \times CO_2$ (comparing Figs. 15b,d). By removing the respective daily seasonal cycle of precipitation from each precipitation dataset using Eq. (1) at each gridpoint, Fig. 15g,h shows the lag-zero composites of the difference between anomalies to the seasonal cycle at $2 \times CO_2$ and $1 \times CO_2$. Active and break events are shown to be more intense against the seasonal cycle, with anomalies increasing in a zonal band across central India and the Bay of Bengal, and increased anomalies of opposite sign also over the southeast equatorial Indian Ocean. Over India, these changes are only statistically significant during monsoon breaks however, indicating that active events at $2 \times CO_2$ are stronger because of the wetter seasonal cycle, while break events have a larger magnitude against the seasonal cycle. During monsoon breaks, the region northeast of India which receives additional precipitation (related to northward movement of the monsoon trough in Krishnamurthy and Shukla, 2007), is increasingly wet.

While there are changes to break event precipitation anomalies for lags of -12 to -8 days (not shown), these are not statistically significant. From around lag$= -6$, break events are significantly drier in the north Bay of Bengal supporting the existing pattern there. Following the event the pattern of break anomaly intensification persists over the north Bay of Bengal, India, Bangladesh and Nepal until at least lag$= +8$.

The above lag-composite analysis has also been carried out based on a precipitation index measured only over the central core region of India (73–82°E, 18–28°N), after Mandke *et al.* (2007). This yields comparable results to the above in terms of projected increases in the intensity of active and break event peaks. In addition, changing the minimum length of events used in construction of the composites (to 3 or 7 days) revealed no major differences.

To summarize changes to precipitation amounts associated with active and break events, we have taken measurements based on Fig. 15 averaged over the central India region (Goswami *et al.*, 2006) as in section 4.1. These are displayed in Table 2. In the $2 \times CO_2$ climate of HadCM3, active and break events are significantly more extreme against the seasonal cycle when compared to $1 \times CO_2$. Active events are also significantly wetter in absolute terms. For break events, however, such absolute changes are statistically insignificant given the increasingly wet mean monsoon. Intensification of the active-break cycles is caused by overall intensification in the hydrological cycle as the available moisture content in the atmosphere is increased, as described in section 4.1. Being dipolar in nature, we speculate that increases in the positive part of the dipole are accompanied by deepening in the other pole, as part of an intensified local Hadley circulation. Hence break events could be more intense against the seasonal cycle because of strengthening convection in the eastern equatorial Indian Ocean, as seen in Figs. 15f,h.

Temporal characteristics of break events such as periodicity and duration could have a dramatic impact on monsoon-affected societies. However, power spectra of precipitation anomaly timeseries over India indicate no significant changes to period at $2 \times CO_2$ (not shown). The mean lengths of active and break events quoted earlier in this section are summarized in Table 3, with the addition of values for $2 \times CO_2$. By design, the use of a normalized index will yield a similar number of days at $1 \times CO_2$ and $2 \times CO_2$, hence at $2 \times CO_2$ the duration of events relative to the $1 \times CO_2$ event thresholds are calculated. The table also shows the mean duration of the longest break event in each season, potentially of more use to society. There are no significant changes to the duration of break events at $2 \times CO_2$ using either measure. For active events, the mean maximum duration is around 2 days longer at $2 \times CO_2$, however given the bias of HadCM3 to longer events than in observations, these difference may be an overestimate. Table 3 shows that re-gridding the observed data to the lower resolution of HadCM3 accounts for only a small proportion of the model bias.

TABLE 3. The mean duration and mean maximum duration of active and break events in HadCM3. Durations at $2 \times CO_2$ are relative to the $1 \times CO_2$-defined level of break event precipitation. Also shown are durations for the raw IMD data, and IMD data interpolated to the model grid (IMD_{N48}). Units are days. In the $2 \times CO_2$ column, an asterisk* denotes a difference from the $1 \times CO_2$ value statistically significant at the 95% level.

threshold	IMD	IMD_{N48}	$1 \times CO_2$	$2 \times CO_2$
mean active	7.0	7.2	9.3	9.9
mean break	7.6	8.3	10.6	12.0
mean max active	7.1	7.5	10.1	12.4*
mean max break	8.0	8.7	12.2	14.0

5. Discussion and conclusions

The greenhouse warming experiment presented here, achieved through the doubling of carbon dioxide concentrations in the atmosphere of the HadCM3 coupled model, has had several impacts on the Indian summer monsoon. Aside from an increase in mean precipitation which seems a robust conclusion among several of the present models, here we have presented future climate changes to subseasonal monsoon behaviour, drawn from century-long integrations, which fall under three main headings. Each of the findings outlined is discussed in the context of various biases inherent in global coupled GCMs.

(*a*) *Spatial changes to subseasonal monsoon rainfall characteristics*

In HadCM3 there is a tendency for a reduction in the number of rain days per season, particularly in the southeast of India. This occurs in conjunction with increased summer mean rainfall intensity, which features the same spatial distribution as changes to mean rainfall. The 95th and 99th percentiles of heavy precipitation on subseasonal timescales are used to measure monsoon extremes and are found to increase quite strongly, although over India itself these changes are only significant over the north, where the probability of achieving the $1 \times CO_2$ levels of precipitation is at least doubled. This suggests a greater potential for damaging floods over the northern region. Changes to extreme precipitation are more marked over the Bay of Bengal, the Indochina peninsula and much of China, although for the latter these changes are from a lower baseline. Increases in heavy precipitation are at the expense of moderate events and are consistent with decreasing number of rain days in some areas. The potential contribution of extreme rainfall events to the seasonal total has been assessed and suggests an increased reliance on these events for water supply, particularly in the southeast where boreal summer rainfall is relatively low and the number of wet days decreases. Such spatial projections as those outlined above must be interpreted carefully, however. One must question the ability of coarse resolution GCMs to simulate the spatial nature of extremes of convection in the monsoon, which featuring large horizontal gradients over regions such as India. In addition, although there is some agreement on greenhouse warming-related increases in the mean summer monsoon over South Asia (Meehl *et al.*, 2007), the spatial pattern of such changes on the regional scale is by no means certain and the results shown here suggest that the spatial pattern of changes to extreme precipitation are strongly tied to projected changes in the mean. Indeed in a study using the Canadian Centre for Climate model (CCC GCM2) at $2 \times CO_2$, Zwiers and Kharin (1998) noted that the strongest change in precipitation extremes occurred over north-west India, related to intensification of the mean monsoon there. Despite such limitations, it is important to stress that the spatial distribution of changes to monsoon extremes depicted here is possible, given the projected mean change found in HadCM3. The authors are currently examining the relationships between spatial patterns of change in mean monsoon rainfall and their associated extremes in the models of the CMIP3 database. Once the whole range of models converge more clearly on the pattern of greenhouse-forced mean monsoon rainfall change and the mechanisms involved, then findings such as those presented here will be more useful. We have also shown that even when measuring average changes over a broad region of central India, large increases in the 95th and 99th percentiles occur.

(*b*) *Changes to the heaviest monsoon rainfall*

To assess the impact of increased greenhouse gas forcing on rainfall extremes over India as a whole, increases in the magnitude of the heaviest precipitation events were measured. Looking at all model data over India and tropics-wide, the increased magnitude of the heaviest rainfall is around

$+13$–14%, in broad agreement with the predicted increase in the water holding capacity of the atmospheric column and the level of surface warming experienced in this model. Thus projected increases in the heaviest rainfall over India seem remarkably predictable. However, models such as HadCM3 are unable to simulate the upper tail of precipitation extremes (Fig. 3b) owing to their resolution. In higher resolution and/or regional climate models, the consequent improved representation of localized deep convection leads to a more realistic (increased) frequency of extreme events (Jones *et al.*, 1997). Consequently, they argue that in higher resolution models, smaller fractional increases are measured in the frequency of upper extremes of precipitation as CO_2 concentrations are increased, together with corresponding larger increases in their magnitude. However the results presented here suggest that HadCM3 has already reached the thermodynamic limit predicted by the Clausius-Clapeyron relation, suggesting that such changes may not be restricted by grid size and are independent of any bias in the seasonal cycle. HadCM3 also lacks a significant dynamic contribution to increase in extremes of monsoon rainfall, given little climate-induced changes to the Somali Jet. Work is in progress to examine if this thermodynamic component is predictable in other coupled GCMs and to elucidate the relative role of any dynamical component. In models which show increases in seasonal mean monsoon rainfall, the Clausius-Clapeyron relation may therefore provide a lower bound on increases in the heaviest rainfall over monsoon regions, supporting the view held by Allen and Ingram (2002).

(*c*) *Changes to active-break cycles*

Break events have been shown to be more intense against the annual cycle in HadCM3 at $2 \times CO_2$, in common with other models ($e.g.$, Mandke *et al.*, 2007). Although these could have important repercussions, particularly for agriculture (heat stress of crops etc.), the fact that their duration and periodicity remain unchanged suggests this may not cause serious problems. More noticeable is the intensification of active events (extended periods of heavy rainfall), which could lead to a greater potential for crop and infrastructure damage as well as loss of life from flooding. The results above are still clear when measured as an average over the central India region. Clearly the ability of GCMs to simulate the intricacies of monsoon intraseasonal oscillations, particularly any biases in their propagation characteristics, is important. We have demonstrated that HadCM3 does have some skill in simulating northward propagation of ISO in the Indian monsoon domain, comparable with other GCMs (Lin *et al.*, 2008). This propagation is still deficient when compared against observed precipitation, likely related to weak air-sea coupled interactions in the model. The representation of such processes could potentially be improved by increasing the atmosphere-ocean coupling frequency and improving the vertical resolution of the upper ocean (Bernie *et al.*, 2005). That HadCM3 at least features some characteristics inherent to monsoon ISO, as well as its mean and seasonal cycle being among the best of the current models (Annamalai *et al.*, 2007), and the large sample size from which these results are drawn, suggests we may have some confidence in the projections of active-break cycles made here. The reasons for the intensification of break events remain unclear, but we speculate that they relate to intensification in the local Hadley circulation, and they remain the subject of a future study.

This paper thus provides a projection of changes to intraseasonal behaviour in the Asian summer monsoon, comprising generally wetter extremes, the upper limit of which seems quite predictable based on the degree of projected warming. Active and break events were found to become more intense against the seasonal cycle. The array of metrics presented will be useful for assessing future, higher resolution GCMs, featuring more realistic ocean-atmosphere coupled processes.

Acknowledgements

A. G. Turner is funded via the EU-ENSEMBLES project, while Julia Slingo is a member of the NERC National Centre for Atmospheric Science (NCAS). The authors are grateful to two anonymous reviewers and the associate editor, Oscar Alves, for their constructive criticism of this work. The India Meteorological Department's gridded rainfall dataset was made available by M. Rajeevan, CMAP was obtained from the Climate Prediction Center, and GPCP data was obtained from the NASA Goddard Space Flight Center. Computing resources were provided by HPCx for running the Unified Model.

References

Adler RF, Huffman GJ, Chang A, Ferraro R, Xie P, Janowiak J, Rudolf B, Schneider U, Curtis S, Bolvin D, Gruber A, Susskind J, Arkin P. 2003. The version 2 global precipitation climatology project (gpcp) monthly precipitation analysis (1979-present). *J. Hydrometeorol.* **4**: 1147–1167. DOI: 10.1175/1525-7541(2003)004<1147:TVGPCP>2.0.CO;2.

Alexander LV, Zhang X, Peterson TC, Caesar J, Gleason B, Klein Tank AMG, Haylock M, Collins D, Trewin B, Rahimzadeh F, Tagipour A, Rupa Kumar K, Revadekar J, Griffiths G, Vincent L, Stephenson DB, Burn J, Aguilar E, Brunet M, Taylor M, New M, Zhai P, Rusticucci M, Vasquez-Aguirre JL. 2006. Global observed changes in daily climate extremes of temperature and precipitation. *J. Geophys. Res.* **111**. DOI:10.1029/2005JD006290.

Allen MR, Ingram WJ. 2002. Constraints on future changes in climate and the hydrologic cycle. *Nature* **419**: 224–232. DOI:10.1038/nature01092.

Annamalai H, Hamilton K, Sperber KR. 2007. The South Asian Summer Monsoon and Its Relationship with ENSO in the IPCC AR4 Simulations. *J. Climate* **20**: 1071–1092. DOI: 10.1175/JCLI4035.1.

Annamalai H, Slingo JM. 2001. Active/break cycles: diagnosis of the intraseasonal variability of the Asian Summer Monsoon. *Clim. Dyn.* **18**: 85–102. DOI:10.1007/s003820100161.

Ashrit R, Douville H, Kumar K. 2003. Response of the Indian Monsoon and ENSO-Monsoon Teleconnection to Enhanced Greenhouse Effect in the CNRM Coupled Model. *J. Meteorol. Soc. Jpn.* **81**: 779–803. DOI: 10.2151/jmsj.81.779.

Bernie DJ, Woolnough SW, Slingo JM, Guilyardi E. 2005. Modelling diurnal and intraseasonal variability of the ocean mixed layer. *J. Climate* **18**: 1190–1202. DOI: 10.1175/JCLI3319.1.

Dai A, Trenberth KE. 2004. The Diurnal Cycle and Its Depiction in the Community Climate System Model. *J. Climate* **17**: 930–951. DOI: 10.1175/1520-0442(2004)017<0930:TDCAID>2.0.CO;2.

Duchon CE. 1979. Lanczos Filtering in One and Two Dimensions. *Journal of Applied Meteorology* **18**: 1016–1022. DOI: 10.1175/1520-0450(1979)018<1016:LFIOAT>2.0.CO;2.

Fu X, Wang B, Li T, McCreary JP. 2003. Coupling between Northward-Propagating, Intraseasonal Oscillations and Sea Surface Temperature in the Indian Ocean. *J. Atmos. Sci.* **60**: 1733–1271. DOI: 10.1175/1520-0469(2003)060<1733:CBNIOA>2.0.CO;2.

Gadgil S, Sajani S. 1998. Monsoon precipitation in the AMIP runs. *Clim. Dyn.* **14**: 659–689. DOI: 10.1007/s003820050248.

Gordon C, Cooper C, Senior CA, Banks H, Gregory JM, Johns TC, Mitchell JFB, Wood RA. 2000. The simulation of SST, sea ice extents and ocean heat transports in a version of the Hadley Centre coupled model without flux adjustments. *Clim. Dyn.* **16**: 147–168. DOI: 10.1007/s003820050010.

Goswami BN, Mohan RSA. 2001. Intraseasonal Oscillations and Interannual Variability of the Indian Summer Monsoon. *J. Climate* **14**: 1180–1198. DOI: 10.1175/1520-0442(2001)014%3C1180:IOAIVO%3E2.0.CO;2.

Goswami BN, Venugopal V, Sengupta D, Madhusoodanan MS, Xavier PK. 2006. Increasing Trend of Extreme Rain Events over India in a Warming Environment. *Science* **314**: 1442–1445. DOI: 10.1126/science.1132027.

Goswami BN, Xavier PK. 2005. Dynamics of ”internal” interannual variability of the Indian summer monsoon in a GCM. *J. Geophys. Res.* **110**. DOI: 10.1029/2005JD006042.

Hennessy KJ, Greogry JM, Mitchell JFB. 1997. Changes in daily precipitation under enhanced greenhouse conditions. *Clim. Dyn.* **13**: 667–680. DOI: 10.1007/s003820050189.

Hu ZZ, Latif M, Roeckner E, Bengtsson L. 2000. Intensified Asian summer monsoon and its variability in a coupled model forced by increasing greenhouse gas concentrations. *Geophys. Res. Lett.* **27**: 2618–2684. DOI: 10.1029/2000GL011550.

Huffman G, Adler RF, Morrissey M, Bolvin DT, Curtis S, Joyce R, McGavock B, Susskind J. 2001. Global precipitation at one-degree daily resolution from multi-satellite observations. *J. Hydrometeor.* **2**: 36–50. DOI: 10.1175/1525-7541(2001)002¡0036:GPAODD¿2.0.CO;2.

Inness P, Slingo J, Woolnough S, Neale R, Pope V. 2001. Organization of tropical convection in a GCM with varying vertical resolution: implications for the simulation of the Madden-Julian Oscillation. *Clim. Dyn.* **17**: 777–793. DOI: 10.1007/s003820000148.

Johns TC, Gregory JM, Ingram WJ, Johnson CE, Jones A, Lowe JA, Mitchell JFB, Roberts DL, Sexton DMH, Stevenson DS, Tett SFB, Woodage MJ. 2003. Anthropogenic climate change for 1860 to 2100 simulated with the HadCM3 model under updated emissions scenarios. *Clim. Dyn.* **20**: 583–612. DOI: 10.1007/s00382-002-0296-y.

Jones RG, Murphy JM, Noguer M, Keen AB. 1997. Simulation of climate change over Europe using a nested regional-climate model. II: Comparison of driving and regional modelling responses to a doubling of carbon dioxide. *Q. J. R. Meteorol. Soc.* **123**: 265–292. DOI: 10.1002/qj.49712353802.

Joseph PV, Simon A. 2005. Weakening trend of the southwest monsoon current through peninsular India from 1950 to the present. *Current Science* **89**: 687–694.

Kemball-Cook S, Wang B. 2001. Equatorial Waves and Air-Sea Interaction in the Boreal Summer Intraseasonal Oscillation. *J. Climate* **14**: 2923–2942. DOI: 10.1175/1520-0442(2001)014<2923:EWAASI>2.0.CO;2.

Kharin VV, Zwiers FW, Zhang X, Hegerl GC. 2007. Changes in Temperature and Precipitation Extremes in the IPCC Ensemble of Global Coupled Model Simulations. *J. Climate* **20**: 1419–1444. DOI: 10.1175/JCLI4066.1.

Kitoh A, Yukimoto S, Noda A, Motoi T. 1997. Simulated Changes in the Asian Summer Monsoon at Times of Increased Atmospheric CO_2. *J. Meteorol. Soc. Jpn.* **75**: 1019–1031.

Krishnamurthy V, Shukla J. 2000. Intraseasonal and Interannual Variability of Rainfall over India. *J. Climate* **13**: 4366–4377. DOI: 10.1175/1520-0442(2000)013<0001:IAIVOR>2.0.CO;2.

Krishnamurthy V, Shukla J. 2007. Intraseasonal and Seasonally Persisting Patterns of Indian Monsoon Rainfall. *J. Climate* **20**: 3–20. DOI: 10.1175/JCLI3981.1.

Krishnamurthy V, Shukla J. 2008. Intraseasonal and Seasonally Persisting Patterns of Indian Monsoon Rainfall. *Clim. Dyn.* **30**: 353–369. DOI: 10.1007/s00382-007-0300-7.

Lal B, Jayanthi N, abd M Rajeevan TP, Devi S, Srivastava AK, Pai DS. 2006. *Monsoon 2005 : A report*. National Climate Centre, Indian Meteorological Department, Pune.

Lin JL, Weickmann KM, Kiladis GN, Mapes BE, Schubert SD, Suarez MJ, Bacmeister JT, Lee MI. 2008. Subseasonal Variability Associated with Asian Summer Monsoon Simulated by 14 IPCC AR4 Coupled GCMs. *J. Climate* **21**: 4541–4567. DOI: 10.1175/2008JCLI1816.1.

Mandke SK, Sahai AK, Shinde MA, Joseph S, Chattopadhyay R. 2007. Simulated changes in active/break spells during the Indian summer monsoon due to enhanced CO_2 concentrations: assessment from selected coupled atmosphere-ocean global climate models. *International Journal of Climatology* **27**: 837–859. DOI: 10.1002/joc.1440.

Martin GM, Arpe K, Chauvin F, Ferranti L, Maynard K, Polcher J, Stephenson DB, Tschuck P. 2000. Simulation of the Asian Summer Monsoon in Five European General Circulation Models. *Atmos. Sci. Let.* **1**: 37–55. DOI: 10.1006/asle.2000.0004.

May W. 2004. Potential future changes in the Indian summer monsoon due to greenhouse warming: analysis of mechanisms in a global time-slice experiment. *Clim. Dyn.* **22**: 389–414. DOI: 10.1007/s00382-003-0389-2.

Meehl G, Collins WD, Boville BA, Kiehl JT, Wigley TML, Arblaster JM. 2000. Response of the NCAR climate system model to increased CO_2 and the role of physical processes. *J. Climate* **13**: 1879–1898. DOI: 10.1175/1520-0442(2000)013<1879:ROTNCS>2.0.CO;2.

Meehl G, Stocker T, Collins W, Friedlingstein P, Gaye A, Gregory J, Kitoh A, Knutti R, Murphy J, Noda A, Raper S, Watterson I, Weaver A, Zhao ZC. 2007. *Global Climate Projections*, ch. 10. Cambridge University Press, pp. 747–846. In: Climate Change 2007: The Physical Science Basis. Contribution of Working Group I to the Fourth Assessment Report of the Intergovernmental Panel on Climate Change. Solomon, S., D. Qin, M. Manning, Z. Chen, M. Marquis, K.B. Averyt, M. Tignor, H.L. Miller (eds.).

Meehl GA, Arblaster JM. 2003. Mechanisms for projected future changes in south Asian monsoon precipitation. *Clim. Dyn.* **21**: 659–675. DOI: 10.1007/s00382-003-0343-3.

Pall P, Allen MR, Stone DA. 2007. Testing the Clausius-Clapeyron constraint on changes in extreme precipitation under CO_2 warming. *Clim. Dyn.* **28**: 351–363. DOI: 10.1007/s00382-006-0180-2.

Perkins SE, Pitman AJ, Holbroock NJ, McAneney J. 2007. Evaluation of the AR4 Climate Models' Simulated Daily Maximum Temperature, Minimum Temperature, and Precipitation over Australia Using Probability Density Functions. *J. Climate* **20**: 4356–4376. DOI: 10.1175/JCLI4253.1.

Pope VD, Gallani ML, Rowntree PR, Stratton RA. 2000. The impact of new physical parametrizations in the Hadley Centre climate model: HadAM3. *Clim. Dyn.* **16**: 123–146. DOI: 10.1007/s003820050009.

Rajeevan M, Bhate J, Kale JD, Lal B. 2006. High resolution daily gridded rainfall data for the Indian region: Analysis of break and active monsoon spells. *Current Science* **91**: 296–306.

Semenov VA, Bengtsson L. 2002. Secular trends in daily precipitation charactersitics: greenhouse gas simulation with a coupled AOGCM. *Clim. Dyn.* **19**: 123–140. DOI: 10.1007/s00382-001-0218-4.

Sen Roy S, Balling Jr RC. 2004. Trends in extreme daily precipitation indices in India. *International Journal of Climatology* **24**: 457–466. DOI: 10.1002/joc.995.

Spencer H, Slingo JM. 2003. The simulation of peak and delayed ENSO teleconnections. *J. Climate* **16**: 1757–1774. DOI: 10.1175/1520-0442(2003)016<1757:TSOPAD>2.0.CO;2.

Sperber KR, Slingo JM, Annamalai H. 2000. Predictability and the relationship between subseasonal and interannual variability during the Asian summer monsoon. *Q. J. R. Meteorol. Soc.* **126**: 2545–2574. DOI: 10.1002/qj.49712656810.

Stephenson DB, Kumar KR, Doblas-Reyes FJ, Royer JF, Chauvin F. 1999. Extreme Daily Rainfall Events and Their Impact on Ensemble Forecasts of the Indian Monsoon. *Mon. Weather Rev.* **127**: 1954–1966. DOI: 10.1175/1520-0493(1999)127<1954:EDREAT>2.0.CO;2.

Sun Y, Solomon S, Dai A, Portman RW. 2006. How often does it rain? *J. Climate* **19**: 916–934. DOI: 10.1175/JCLI3672.1.

Sun Y, Solomon S, Dai A, Portman RW. 2007. How often will it rain? *J. Climate* **20**: 4801–4818. DOI: 10.1175/JCLI4263.1.

Trenberth KE, Dai A, Rasmussen RM, Parsons DB. 2003. The changing character of precipitation. *Bull. Am. Meteorol. Soc.* **September**: 1205–1217. DOI: 10.1175/BAMS-84-9-1205.

Turner AG, Inness PM, Slingo JM. 2005. The role of the basic state in the ENSO-monsoon relationship and implications for predictability. *Q. J. R. Meteorol. Soc.* **131**: 781–804. DOI: 10.1256/qj.04.70.

Turner AG, Inness PM, Slingo JM. 2007. The effect of doubled CO_2 and model basic state biases on the monsoon-ENSO system. I: Mean response and interannual variability. *Q. J. R. Meteorol. Soc.* **133**: 1143–1157. DOI: 10.1002/qj.82.

Vecchi GA, Harrison DE. 2002. Monsoon Breaks and Subseasonal Sea Surface Temperature Variability in the Bay of Bengal. *J. Climate* **15**: 1485–1493. DOI: 10.1175/1520-0442(2002)015¡1485:MBASSS¿2.0.CO;2.

Webster PJ, Magana VO, Palmer TM, Shukla J, Tomas RA, Yanai M, Yasunari T. 1998. Monsoons: Processes, predictability, and prospects for predcition. *J. Geophys. Res.* **103**: 14 451–14 510. DOI: 10.1029/97JC02719.

Xie P, Arkin PA. 1997. Global Precipitation: A 17-Year Monthly Analysis Based on Gauge Observations, Satellite Estimates, and Numerical Model Outputs. *Bull. Am. Meteorol. Soc.* **78**: 2539–2559. 10.1175/1520-0477(1997)078<2539:GPAYMA>2.0.CO;2.

Zwiers FW, Kharin VV. 1998. Changes in the Extremes of the Climate Simulated by CCC GCM2 under CO_2 Doubling. *J. Climate* **11**: 2200–2222. DOI: 10.1175/1520-0442(1998)011<2200:CITEOT>2.0.CO;2.